Micrometre-sized In₂S₃ half-shells by a new dynamic soft template route: properties and applications

Peng Gao[1], **Yi Xie**[1,2,4], **Shaowei Chen**[3] **and Mingzhou Zhou**[1]

[1] Nano-materials and Nano-chemistry, Hefei National Laboratory for Physical Sciences at Microscale, University of Science and Technology of China, Hefei, Anhui 230026, People's Republic of China
[2] School of Chemical and Material Engineering, Southern Yangtze University, Wuxi, Jiangsu 214036, People's Republic of China
[3] University of California, Santa Cruz, CA 95064, USA

E-mail: yxielab@ustc.edu.cn

Abstract
A novel dynamic soft template solution route has been developed for the preparation of micrometre-sized In₂S₃ half-shells, assembled by fine nanoparticles. This novel half-shell nanostructure was characterized by electron microscopes, x-ray diffraction (XRD), x-ray photoelectron (XPS), and optical spectroscopes. The catalytic property in the electro-oxidation of the nitric oxide (NO) of the half-shells was also investigated, which could be drastically enhanced by the loading of Ag nanoparticles. Finally, the template-free, one-pot method described here is likely to be useful in the preparation of many other half-shell structures.

1. Introduction

Hollow nanostructures are particularly interesting for applications as confined reaction vessels (e.g., for (bio-) chemistry performed with single molecules or biomimetic mineralization), drug carriers, or protective shells for enzymes or catalysts [1–3]. These hollow structures, which normally consist of inorganic materials such as metals, metal oxides or metal chalcogenides, provide both chemical functionality and designable inner space for meeting new technological challenges. Of these, half-shells have three useful properties because of their unique geometries: (i) a high ratio of surface area to volume, (ii) a large length of edge relative to size, and (iii) an entropic resistance to assembling into close-packed structures. Half-shells of gold, platinum, and palladium have been fabricated only through the colloidal template method, in which the metal films were deposited onto the silica template or polystyrene particle template [4, 5]. Among various preparation methods for the nanomaterials, solution methods offer a high degree of preparative flexibility, and this synthetic route is predestined to facilitate the development of a future nanotechnology, because it provides control of particle size

and gives access to kinetically stable phases [6, 7]. To the best of our knowledge, this is the first report found in the literature that is related to the synthesis of nanoscale half-shells through solution methods.

In this paper, we designed a novel dynamic soft template method in a metastable water–DMS (dimethyl sulfide) solution system to synthesize half-shell architecture. Considering the hollow structure we expect, the emulsion system is surely an appropriate system to supply an interface for the nanoparticles to assemble on, which has been widely applied in the formation of hollow spherical structures of inorganic materials [8]. Emulsions are the dispersions of two immiscible liquids. Oil-in-water (o/w) emulsions refer to dispersions of oil droplets in an aqueous continuous phase and water-in-oil (w/o) emulsions to dispersions of aqueous droplets in a continuous oil-type base. With the appropriate adjustment of experiment parameters and by formation of small enough droplets (typically around or below 1 μm), good stability over a prolonged time period under certain conditions can be achieved. In the stable o/w system, the oil droplets tend to shrink together to form various conformations of molecular assemblies to minimize the free energy and different unique micelle-like aggregations can be formed under different

compositional and operational conditions, such as cylindrical, hexagonal, cubic, lamellar, and spherical conformations. Similar to surfactants in organic solvents or low molecular weight polymer in water, the component concentrations and the system temperature dramatically affect and alter the morphology of molecular aggregation, for instance, from lamellar aggregation to spherical micelle-like aggregation under certain conditions. Controlling the reaction parameters and slowing the transformation may provide the molecular aggregations with special morphology for the nanoparticle growth. Enlightened by the synthesis of carbon nanotubes prepared by curling the graphite layers, it is cognized that the precursors with lamellar structure could be turned into shells of hollow structures. Moreover, metastable lamellar molecular aggregations are usually formed and inflected depending on the surface tensions in the emulsion systems. Accompanied by reducing the surface tensions and slowly changing the ratio of the water phase and oil phase, the metastable lamellar molecular aggregations will tend to wrap up. Thereby, a 'layer to half-shell' route emerges, and the experiment result successfully proves the feasibility of this method.

In this work, tetragonal indium sulfide was selected as an example, due to its exciting optoelectronic properties, such as being an n-type semiconductor with a medium energy gap of 2.00 eV [9–15], arising from its defect structures. The subtle electronic properties suggest that it has the ability to promote electron transfer reaction when used as an electrode in electrochemical reactions similar to carbon nanotubes [16]; however, this has not been studied before. In this paper we successfully prepared In$_2$S$_3$ half-shell structures and find that such In$_2$S$_3$ half-shell structures are excellent catalyst supporters in which targeted catalysts can be easily loaded. For instance, nanocrystalline Ag is selected as the targeted catalyst for the electro-oxidation of nitric oxide (NO), due to its importance in biology [17–24]. The results indicate that the half-shells not only act as the catalyst supporter, but have the prominent cooperating catalytic effect toward the electrochemical oxidation of NO, which demonstrate that the composites with half-shell supporter are superior electrode materials and can be used as electrochemical sensors to detect directly NO in aqueous solutions.

2. Experimental details

2.1. Preparation of In$_2$S$_3$ half-shells

In a typical reaction, InCl$_3$ (2 mmol) and 20 ml dimethyl sulfoxide (DMSO) were added into a 25 ml Teflon-lined autoclave, which was then filled with 5 ml 75% aqueous hydrazine. The autoclave was sealed and maintained at 180 °C for 48 h and then cooled to room temperature naturally. The precipitate was filtered off and washed with distilled water and absolute ethanol several times.

2.2. Preparation of Ag/In$_2$S$_3$ nanocomposites

2 mmol as-prepared In$_2$S$_3$ and 2 mmol AgNO$_3$ were added into 100 ml anhydrous alcohol solution. Then the system was put in the dark and stirred for three days. The product was then collected and filtered with the porous poly(tetrafluoroethene) (the average diameter of the holes is about 200 nm).

2.3. Preparation of standard NO solution

NO standards were prepared by serial dilution of a saturated NO solution. Preparation of the saturated NO solutions involved meticulous exclusion of O$_2$, as NO could be rapidly destroyed by O$_2$. To produce NO-saturated solutions, deionized water solutions (10 ml) were bubbled with nitrogen for 30 min to remove oxygen. Then the solution was bubbled with pure NO gas (Aldrich) for 30 min and kept under a NO atmosphere prior to use. Standards were made fresh for each experiment and kept in a glass flask with a rubber septum. The aqueous NO-saturated solution has a NO concentration of 1.8 mM at 20 °C [25]. Dilutions of the saturated solution were made using deoxygenated water samples. A gas-tight syringe was used to transfer the NO solution.

2.4. Fabrication of the modified electrodes

Prior to modification, the bare glassy carbon electrode (GCE) (4 mm diameter) was polished successively with 6, 1 and 0.05 μm α-alumina slurries on a polishing pad. Then it was rinsed with doubly distilled water, and sonicated in ethanol and doubly distilled water for 5 min, respectively. It was dried with high purity nitrogen immediately before use.

The as-prepared Ag/In$_2$S$_3$ nanocomposites (100 mg) were dispersed in 10 ml anhydrous alcohol under sonication for 30 min. A 5 μl aliquot of this dispersion solution was dropped onto the surface of the GCE and dried in air at room temperature. Then, the Ag/In$_2$S$_3$ nanocomposite modified electrode was obtained and denoted as In$_2$S$_3$–Ag/GCE. The In$_2$S$_3$/GCE and Ag/GCE were prepared by dropping dispersion solutions of In$_2$S$_3$ and Ag nanoparticles on bare GCE as mentioned above, respectively.

2.5. Apparatus

Cyclic voltammetry (CV) experiments were performed with a CHI 660 electrochemical workstation (ChenHua Instruments Co., Shanghai, China). A conventional three-electrode system was used, consisting of a bare or modified glassy carbon (4 mm diameter) working electrode (GCE), platinum wire auxiliary electrode and a saturated calomel reference electrode (SCE). All experiments were carried out at 20 ± 1 °C. X-ray powder diffraction (XRD) analysis was carried out with a Japan Rigaku D/max-rA x-ray diffractometer with graphite monochromatized Cu Kα radiation (λ = 1.541 78 Å). The scan rate of 0.05° s^{-1} was used to record the patterns in the 2θ range of 20°–70°. A transmission electron microscopy (TEM) image and electron diffraction (ED) were taken on a Hitachi model H-800 transmission electron microscope with an accelerating voltage of 200 kV. Scanning electron microscopy (SEM) was performed on an X-650 scanning electron microanalyser. A field emission scanning electron microscope (FE-SEM) image was obtained on a JSM-6700F field emission scanning electron microanalyser (JEOL, Japan). X-ray photoelectron spectroscopy (XPS) was performed on an ESCALab MKII x-ray photoelectron spectrometer, using Mg Kα x-ray as the excitation source. The binding energies obtained in the XPS analysis were calibrated against the C 1s peak at 284.2 eV. UV–vis absorption spectroscopy was performed on a JGNA Specord 200 PC
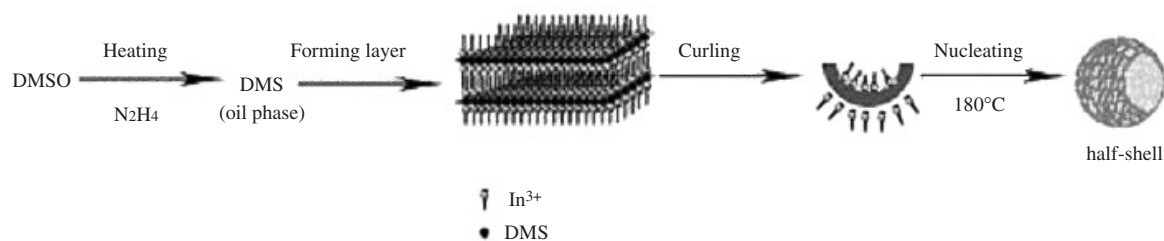
Scheme 1. Schematic illustration of the 'layer to half-shell' growing process of the In$_2$S$_3$ half-shells.

UV–vis spectrophotometer when ethanol was used as a reference. Photoluminescence experiments were carried out on a model LS-55 fluorescence spectrometer from Perkin Elmer Corporation with a Xe lamp at room temperature.

3. Results and discussion

Before discussing the experimental results, we will introduce our general strategy for the synthesis of In$_2$S$_3$ half-shells.

The traditional droplet size-reducing steps involved during preparation in emulsion systems include constant mild stirring using a magnetic stirrer when initially mixing oil and water phases and the final droplet-size homogenization using a two-stage homogenizer valve assembly. However, these conditions are difficult to realize in the Teflon-lined autoclave, in which In$_2$S$_3$ nanoparticles can be prepared under mild temperature and in an airtight system. In order to provide a homogeneous o/w emulsion system for preparing In$_2$S$_3$ half-shells, DMSO and aqueous hydrazine were selected as the initial solvents, because DMSO would be deoxidized to dimethyl sulfide (DMS) in the alkaline and reductive solution at higher temperature [28]. Furthermore, the DMS droplets (oil phase) engendered from the initial solution would disperse homogeneously in the final aqueous solution. At the same time, controlling the reaction temperature and slowing the reaction speed could provide a metastable o/w system, in which the DMS molecular aggregations underwent a shrinking evolution, as shown in scheme 1.

Typical TEM images and SEM images of the as-prepared product are shown in figure 1, in which one can see that the products all exhibit hollow hemispherical shell patterns with an obvious coiling at the open side. These half-shells have diameters ranging from 2 to 4 μm, and most of the products are about 2 μm in diameter. The thickness of the shells is difficult to examine for the curled edge, but it is obvious that the shells are very thin and composed of homogeneous nanocrystals. The ED image (inset in figure 1(A)) also indicates that the half-shells are composed of tiny nanocrystals. Figure 1(D) shows the XRD pattern of the as-prepared product. All the peaks could be indexed to the tetragonal In$_2$S$_3$ phase with lattice parameters $a = 7.617$ Å, $c = 32.320$ Å, in agreement with the reported data of $a = 7.619$ Å, $c = 32.329$ Å (JCPDS Card Files, 25–390). No characteristic peaks were observed for other impurities such as In$_2$O$_3$, S or In(OH)$_3$. The average size of the products is roughly calculated by Scherrer's equation to be 20 nm, which also indicates the structures are composed of tiny nanocrystals.
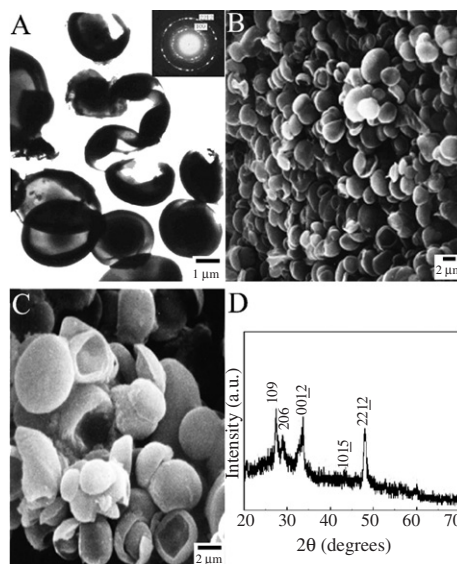
Figure 1. (A) TEM images of half-shells of In$_2$S$_3$; the inset is the ED pattern from one half-shell. (B) Low magnification SEM images of the as-obtained half-shells. (C) High magnification SEM images of the half-shells. (D) XRD pattern for the half-shells.

Further evidence for the quality and composition of the samples was obtained by XPS of the products. In the XPS analysis the binding energies obtained were corrected for specimen charging by referencing the C 1s to 284.20 eV. The In 3D core level spectrum (figure 2(A)) shows the observed value of the binding energies for In 3d$_{5/2}$ (443.6 eV) agree well with the reported data in In$_2$S$_3$ (444.3 eV) [26]. The S 2p$_{3/2}$ binding energy of In$_2$S$_3$ (figure 2(B)), centred at 160.6 eV, is very consistent with those observed in chalcopyrite CuFeS$_2$ [27].

In order to check the growth process of the half-shells, TEM examinations of the products with different reaction times are performed, as shown in figure 3. It is obvious that the products change from lamellar structure to the coiling half-shell structure in the reaction process. The TEM images (figure 3(A) and inset in figure 3(B)) also show clearly that the lamellar structures and the half-shells are composed of tiny nanoparticles.

In this approach, DMSO is first deoxidized by the reducing agent N$_2$H$_4$ to dimethyl sulfide (DMS) [28], which forms the oil phase in the solution. This process is slow at the beginning of heating stage at lower temperatures. When the amount of DMS in the aqueous solution reaches an optimal proportion, lamellar aggregations of DMS form. In^{3+} in the solution is attracted by the S atom of DMS and disperses in the space of
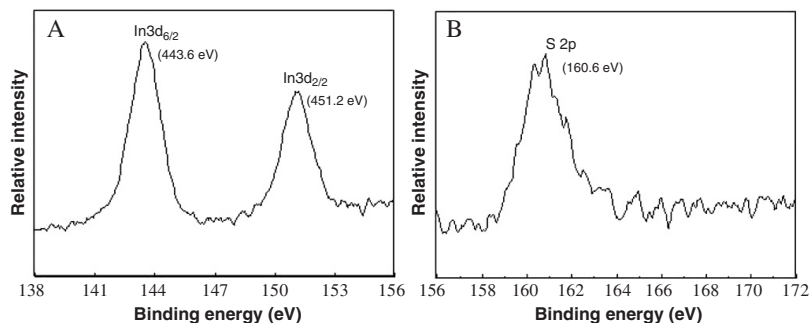
Figure 2. XPS spectra of the sample: (A) In 3d region, (B) S 2p region.
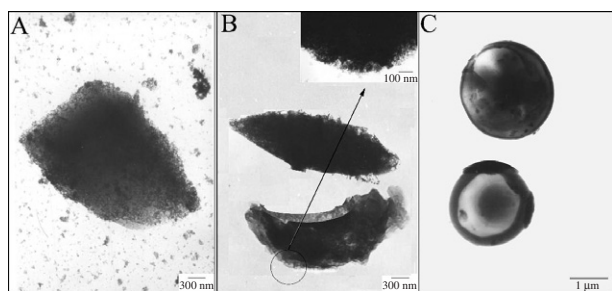

Figure 3. TEM images of the products reacted for different times: (A) 1 h, (B) 2 h and (C) 6 h, which obviously display the 'layer to half-shell' growing process.

Figure 4. UV–vis spectra of the In$_2$S$_3$ half-shells.

Figure 5. Room temperature PL spectrum of the sample.

the lamellar structures, as shown in figure 3(A). At the same time, In^{3+} combines with S atoms of DMS, which decreases the amount of DMS continuously. The resulting decrease and the increase of the amount of DMS from the deoxidized DMSO bring the system into a dynamic balance. However, the quantity of DMS is abundant, and the gradual increase of the amount of DMS changes the ratio of water phase and oil phase. Accompanied by slowly changing the ratio of the water phase and oil phase, in order to reduce the surface tensions, the metastable lamellar molecular aggregations will tend to wrap up. So the lamellar structure curls and transfers into the hemispherical structure, as shown in figure 3(B). Thus the In$_2$S$_3$ half-shells are formed. The whole process is illustrated diagrammatically in scheme 1.

In this reaction, the temperature plays an important role. It accelerates the deoxidization of DMSO, which provides the postulate for the formation of the o/w system. It is also the necessary factor for the nucleation and growth of In$_2$S$_3$ half-shells. In the similar reactions with lower temperatures (120–160 °C), only poorly crystallized In$_2$S$_3$ half-shells could be obtained. In the similar reactions with higher temperatures, the increase of the amount of DMS becomes so fast as to destroy the dynamic balance completely, which makes the structure transformation of the molecular aggregation impossible. So the proper w/o or o/w system and the effective kinetic controlling means for the different objects are the crux for the preparation of hollow hemispherical shells.

The optical property of the In$_2$S$_3$ half-shells is studied through UV–vis spectroscopy and PL excitation spectrum. The result of UV–vis spectroscopy (figure 4) shows that there is an obvious absorption band at 266 (4.66 eV), which should
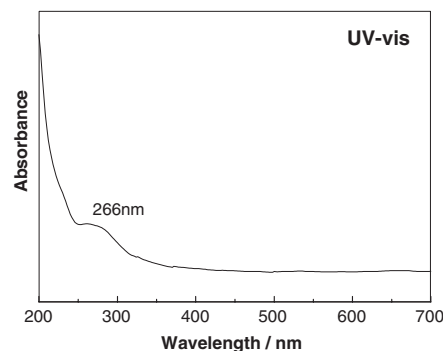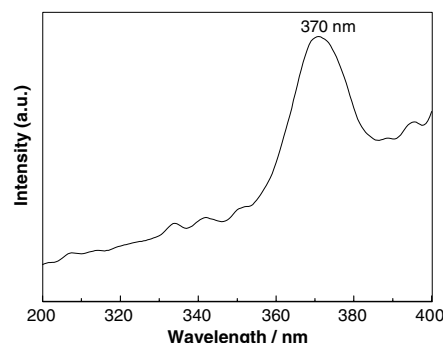
be attributed to the valence-to-conduction-band transition in indium sulfide.

The PL excitation spectrum of the In$_2$S$_3$ half-shells is shown in figure 5. Under PL excitation at 216 nm, the In$_2$S$_3$ half-shells emit blue light at 370 nm (corresponding to 3.35 eV). It clearly indicates the existence of electronic transition at a particular wavelength (370 nm), and is stronger than that in the bulk In$_2$S$_3$, which is virtually non-luminescent. Both the results of UV–vis spectra and PL spectra indicate that the products are composed of tiny nanocrystals, which is in agreement with the result of the XRD analysis and the ED result. By comparing them with the previous results of UV–vis spectra and PL spectra for the nanocrystalline In$_2$S$_3$ [29], it was found that the results are similar to the results of the 20 nm sized In$_2$S$_3$ nanoparticles. This also indicates that the size of the nanoparticles rather than their hemispherical structure take full responsibility for the blue shift.
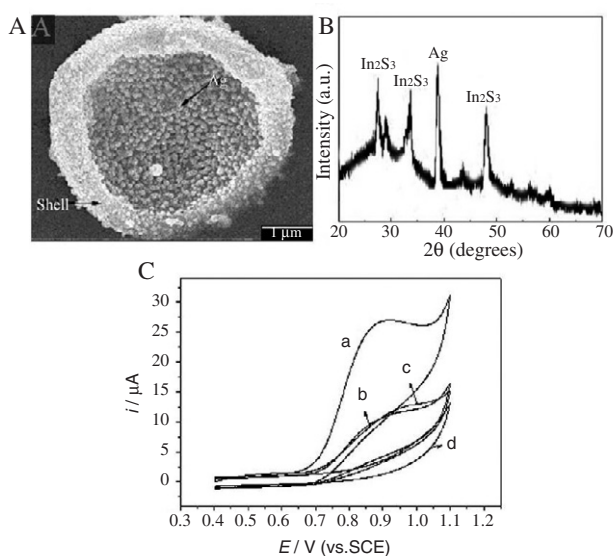
Figure 6. (A) FE-SEM image of In$_2$S$_3$–Ag nanocomposite. (B) XRD pattern of In$_2$S$_3$–Ag nanocomposite. (C) Cyclic voltammograms of In$_2$S$_3$–Ag/GCE (a), In$_2$S$_3$/GCE (b), and Ag/GCE (c) in the presence of 1.64×10^{-4} M NO and bare GCE (d) in 0.1 M PBS (pH 7.4) at 20 mV s^{-1}. The electrode area is 12.6 mm^2.

Due to their central hollow cores and the outside walls, the half-shells can be used as a superior supporter to store catalytic materials, such as noble metal catalysts. This special structure makes the loading and releasing process very simple and the recycling of the catalysts becomes easy. Figure 6(A) is the FE-SEM image of the as-prepared nanocomposites with supported Ag nanoparticles. The size of the silver nanoparticles is about 100 nm. In order to examine the phase and purity of as-prepared nanocomposites, x-ray diffraction (XRD) was conducted, as shown in figure 6(B), which proved that the nanocomposites are composed with In$_2$S$_3$ and Ag. Figure 6(C) shows the cyclic voltammetric responses of In$_2$S$_3$–Ag/GCE (a), In$_2$S$_3$/GCE (b) and Ag/GCE (c) in the presence of 1.64×10^{-4} M NO. A remarkable increase of oxidation current and reduction of overpotential can be seen at In$_2$S$_3$–Ag/GCE (curve (d)), with a peak potential of about 0.89 V, which corresponds to the direct oxidation of NO to NO^{3-} [30]. This potential is about 50 and 90 mV more negative than the oxidation peak at the In$_2$S$_3$/GCE (figure 6(C)(b)) and Ag/GCE (figure 6(C)(c)), respectively. The In$_2$S$_3$–Ag/GCE could further reduce the overpotential and enhance the current response of NO oxidation over the individual In$_2$S$_3$/GCE (figure 6(C)(b)) or Ag/GCE (figure 6(C)(c)), which demonstrated the cooperative effect of In$_2$S$_3$ and Ag in the electrocatalytic oxidation of NO. It should be noted that the GCE modified by the pure In$_2$S$_3$ alone could also catalyse the oxidation of NO to a certain extent, an observation not reported before in the literature. Significantly, it was also found that the composite catalysts are very stable in ambient air, with almost no decrease of current for one month.

4. Conclusions

In summary, we have developed an effective route for the synthesis of mesoscale half-shells of tetragonal indium

sulfide. These half-shells were subject to extensive structural characterization by electron microscopes, x-ray diffraction (XRD), x-ray photoelectron (XPS) and optical spectroscopes. The In$_2$S$_3$ half-shells could act as excellent catalyst supporters, in which targeted catalysts, such as nanocrystalline Ag, were easily loaded and formed In$_2$S$_3$–Ag nanocomposite catalyst, showing a drastic enhancement in the electrocatalytic oxidation of NO as compared to that of as-prepared In$_2$S$_3$ half-shells. We believe that the principle of using the protective ability of the nanocontainers in combination with these open gated pores will have potential applications in many areas, such as sensor technology, diagnostics, catalysis, and so forth.

References

[1] Chiu D T *et al* 1999 *Chem. Phys.* **247** 133
[2] Meier W 2000 *Chem. Soc. Rev.* **5** 295
[3] Caruso F 2001 *Adv. Mater.* **13** 11
[4] Love J C, Gates B D, Wolfe D B, Paul K E and Whitesides G M 2002 *Nano Lett.* **2** 891
[5] Liu J Q, Maaroof A I, Wieczorek L and Cortie M B 2005 *Adv. Mater.* **17** 1276
[6] Walton R I 2002 *Chem. Soc. Rev.* **31** 230
[7] Byrappa K and Yoshimura M 2001 *Handbook of Hydrothermal Technology* (NY, USA: William Andrew Publishing)
[8] Huang J and Xie Y 2000 *Adv. Mater.* **11** 808
[9] Rehwald W and Harbeke G 1965 *J. Phys. Chem. Solids* **26** 1309
[10] Gilles J M, Hatwell H, Offergeld G and van Cakenberghe J 1962 *Phys. Status Solidi* b **2** 73
[11] Kim W T and Kim C D 1986 *J. Appl. Phys.* **60** 2631
[12] Nomura R, Inazawa S, Kanaya K and Matsuda H 1989 *Appl. Organomet. Chem.* **3** 195
[13] Kamoun N, Belgacem S, Amlouk M, Bennaceur R, Bonnet J, Touhari F, Nouaoura M and Lassabatere L 2001 *J. Appl. Phys.* **89** 2766
[14] El Shazly A A, Abd Elhady D, Metwally H S and Seyam M A M 1998 *J. Phys.: Condens. Matter* **10** 5943
[15] Choe S H, Bang T H, Kim N O, Kim H G, Lee C I, Jin M S, Oh S K and Kim W T 2001 *Semicond. Sci. Technol.* **16** 98
[16] Nugent J M, Santhanam K S V, Rubio A and Ajayan P M 2001 *Nano Lett.* **1** 87
[17] Murad F 1999 *Angew. Chem. Int. Edn* **38** 1856
[18] Furchgott R F 1999 *Angew. Chem. Int. Edn* **38** 1870
[19] Palmer R M J, Ferrige A G and Moncada S 1987 *Nature* **327** 524
[20] Schuman E M and Madison D V 1991 *Science* **254** 1503
[21] Hibbs J B, Vavrin Z Jr and Tainton R R 1987 *J. Immunol.* **138** 550
[22] Maskus M, Pariente F, Wu Q, Toffanin A, Shapleigh J P and Abruňa H D 1996 *Anal. Chem.* **68** 3128
[23] Trévin S and Bedioui F 1996 *J. Devynck. Talanta* **43** 303
[24] Trévin S, Bedioui F and Devynck J 1996 *J. Electroanal. Chem.* **408** 261
[25] Butler A R and Williams D L H 1993 *Chem. Soc. Rev.* **22** 233
[26] Wanger C D, Riggs W M, Davis L E, Moulder J F and Muilenberg G E 1978 *Handbook of X-Ray Photoelectron Spectroscopy* (MA, USA: Perkin–Elmer Corporation (Physical Electronics))
[27] Nakai I, Sugitani Y, Nagashima K and Niwa Y 1978 *J. Inorg. Nucl. Chem.* **40** 789
[28] Zinder S H and Brock T D 1978 *J. Gen. Microbiol.* **105** 335
[29] Xiong Y and Xie Y 2002 *J. Mater. Chem.* **12** 98
[30] Zhang X, Cardosa L and Broderick M 2000 *Electroanalysis* **14** 12